Therapeutic Pretargeting with Gold Nanoparticles as Drug Candidates for Boron Neutron Capture Therapy

Irene V. J. Feiner,[a] Krishna R. Pulagam,[a] Vanessa Gómez-Vallejo,[a] Kepa Zamacola,[a] Zuriñe Baz,[a] María M. Caffarel,[b,c] Charles H. Lawrie,[b,c,d] Ane Ruiz-de-Angulo,[e] Mónica Carril,[c,f,g]

Jordi Llop [a,h,†]

[a] CIC biomaGUNE, Basque Research and Technology Alliance (BRTA), Paseo Miramon 182, 20014, San Sebastian, Spain.

[b] Biodonostia Health Research Institute, San Sebastian, Spain.

[c] IKERBASQUE, Basque Foundation for Science, Bilbao, Spain.

[d] Radcliffe Department of Medicine, University of Oxford, Oxford, UK.

[e] CIC bioGUNE, Basque Research and Technology Alliance (BRTA), Building 801A, 48160 Derio, Spain

[f] Instituto Biofisika UPV/EHU, CSIC, Barrio Sarriena s/n, E-48940, Leioa, Bizkaia, Spain

[g] Departamento de Bioquímica y Biología Molecular, UPV/EHU, Barrio Sarriena s/n, E-48940, Leioa, Bizkaia, Spain

[h] Centro de Investigación Biomédica en Red – Enfermedades Respiratorias (CIBERES).

Corresponding author

†Jordi Llop; Paseo Miramón 182, 20014 San Sebastián, Guipúzcoa, Spain. E-mail: jllop@cicbiomagune.es; Phone number: +34 943 005 333

Abstract

Boron neutron capture therapy (BNCT) is a binary approach for cancer treatment in which boron-10 atoms and thermal neutrons need to co-localize to become effective. Recent research in the development of BNCT drug candidates focuses increasingly on nanomaterials, with the advantages of high boron loadings and passive targeting due to the enhanced permeability and retention (EPR) effect. We propose the use of small boron-rich gold nanoparticles (AuNPs) in combination with a pretargeting approach. Small sized polyethylene glycol-stabilized AuNPs (core size 4.1±1.5 nm), were synthesized and functionalized with thiolated cobalt *bis*(dicarbollide) and tetrazine. To enable *in vivo* tracking of the AuNPs by positron emission tomography (PET), the core was doped with $[^{64}Cu]CuCl_2$. For the pretargeting approach, the monoclonal antibody Trastuzumab was functionalized with *trans*-cyclooctene-*N*-hydroxysuccinimide ester. After proving *in vitro* occurrence of the antibody conjugation onto the AuNPs by click reaction and the low toxicity of the AuNPs, the boron delivery system was evaluated *in vivo* using breast cancer xenograft bearing mice and PET imaging. Tumor uptake due to the EPR effect could be witnessed with ca. 5 %ID/cm^3 at 24 h post injection, but with slower clearance than expected. Therefore, no increased retention could be observed using the pretargeting strategy.

Keywords

Gold nanoparticles, pretargeting, BNCT, PET, nuclear imaging

1. Introduction

Cancer remains one of the leading causes of death worldwide.[1] In spite of recent advances, the development of therapeutic strategies capable to selectively actuate in the tumor while sparing healthy organs and tissues is urgently required. Boron

neutron capture therapy (BNCT),[2] a binary approach to cancer therapy in which two non-toxic components need to co-localize to become effective, fulfills this criterion. In BNCT, Boron-10 (^{10}B) atoms selectively delivered to tumor tissue are irradiated with neutrons. The interaction of the incident neutrons with the stable ^{10}B atoms triggers a nuclear reaction which results in the formation of recoil lithium ions and α-particles. These have high linear energy transfer (LET) and a range within the diameter of a single cell (5-9 µm),[3] generating thus localized cellular damage which results in tumor-cell death.

Although BNCT was first proposed more than 80 years ago,[2] only two boronated compounds are currently used in clinical trials: (L)-4-dihydroxy-borylphenylalanine, commonly known as boronophenylalanine (BPA); and sodium mercaptoundecahydro-closo-dodecaborate, commonly known as sodium borocaptate (BSH).[4] These, however, show low tumor selectivity and are efficacious only in some cancer types. The lack of success in the development of promising drug candidates, together with the inconvenience of conducting clinical trials close to nuclear reactors, temporarily discouraged the development of BNCT. However, two major advances have opened new avenues for this promising therapeutic modality: first, the development of biomedical cyclotrons capable to generate high intensity neutron beams,[5] which enable treating patients in a friendly environment and at lower cost; second, the emergence of nanotechnology, which has provided the possibility of boron-rich nanomedicines capable to passively accumulate in tumor tissue by taking advantage of the enhance permeability and retention (EPR) effect. As a result, nano-sized materials including liposomes,[6] iron oxide nanoparticles,[7] carbon[8] and boron nitride[9] nanotubes, and gold nanoparticles,[10] among others, have been proposed, synthesized and eventually evaluated as boron carriers.

The size of the nanomaterials, together with surface charge and functionalization, plays a pivotal role in their biodistribution after intravenous administration, and severely affects the degree of accumulation in the tumor. In general terms, large particles show slow distribution with accumulation in organs with high presence of the mononuclear phagocytic system (MPS) such as the liver, the spleen and the lungs, which may cause local toxicity and undesired side effects. Contrarily, ultra-small particles below the glomerular filtration threshold of the kidneys (ca. 8 nm) are likely to be rapidly eliminated via urine.[11] Hence, they are less prone to show localized off-target toxicity, although bioavailability and hence tumor accumulation are severely compromised.

In the pursuit of a therapeutic strategy capable of achieving high tumor accumulation and fast clearance, we recently introduced a pretargeting strategy (Figure 1a),[12] previously applied in the fields of nuclear imaging and radiation therapy.[13] In our approach, a tumor targeting, *trans*-cyclooctene (TCO) functionalized monoclonal antibody (mAb) was administered first. After accumulation in tumor tissue and clearing from blood (24 h), tetrazine (Tz)-functionalized boron-rich carbon-based nanoparticles (particle diameter = 3-10 nm) were injected. The on-site click reaction between the TCO-mAb and the Tz-functionalized nanoparticles led to enhanced tumor retention when compared to the nanoparticles injected alone, without pre-injection of the antibody. In spite of the positive results, maximum nanoparticle uptake in the tumor was ca. 3 % of injected dose per gram (%ID/g), mainly due to the extremely fast clearance of the nanoparticles. These results suggested the need for developing other boron-rich nano-platforms with slower clearance. Among all alternatives, gold nanoparticles are particularly interesting, as gold is chemically inert and non-toxic, both shape and size can be easily tuned and surface properties and

functionalization can be easily modulated due to the well-defined surface chemistry of gold.[14]

Herein, we report the synthesis, characterization and *in vivo* evaluation of boron-rich gold nanoparticles using a pretargeting strategy. Based on our previous works,[10b] we synthesized small-sized gold nanoparticles (AuNPs; core size = 4.1 ± 1.5 nm) stabilized with polyethylene glycol and bearing cobalt *bis*[dicarbollide] (COSAN) units and Tz moieties on the surface (Figure 1b). Successful radiolabeling could be achieved by incorporation of the positron emitter copper-64 (^{64}Cu) within the gold core. The capacity of the newly developed nanosystem to selectively accumulate in the tumor *via* EPR effect, combined with a pretargeting strategy, was finally evaluated in a xenograft mouse model of breast cancer using PET imaging.
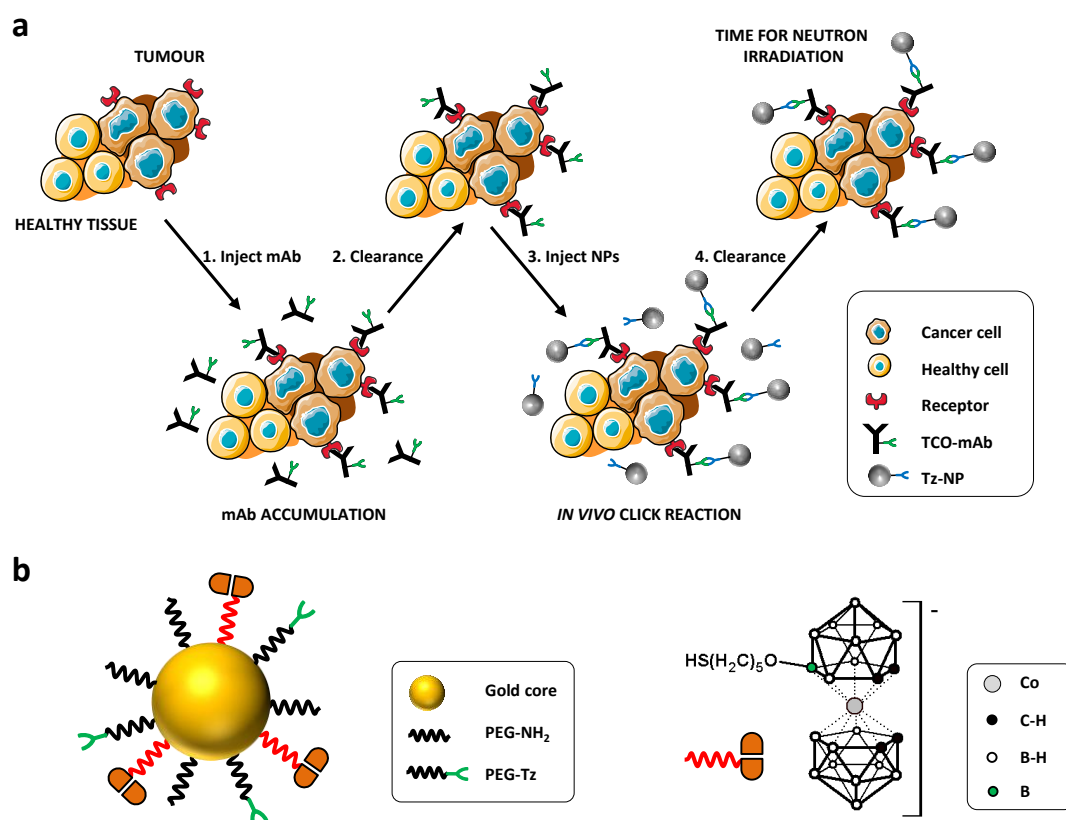
Figure 1: a) Schematic representation of the pretargeting strategy using small boron-rich nanoparticles (NPs). The TCO-functionalized antibody (TCO-mAb) accumulates

in the tumor (1). After clearance (2), boron-rich, tetrazine functionalized NPs (3) are injected. Those reaching the tumor undergo bioorthogonal click reaction and are selectively retained, while non-reacted particles are cleared (4). At the final stage, neutron irradiation can be applied; b) schematic representation of a small, spherical gold nanoparticle stabilized with polyethylene glycol (PEG) and functionalized with tetrazine (Tz) and thiolated cobalt *bis*(dicarbollide) (COSAN-SH); chemical structure of COSAN-SH is shown on the right.

2. Results and discussion

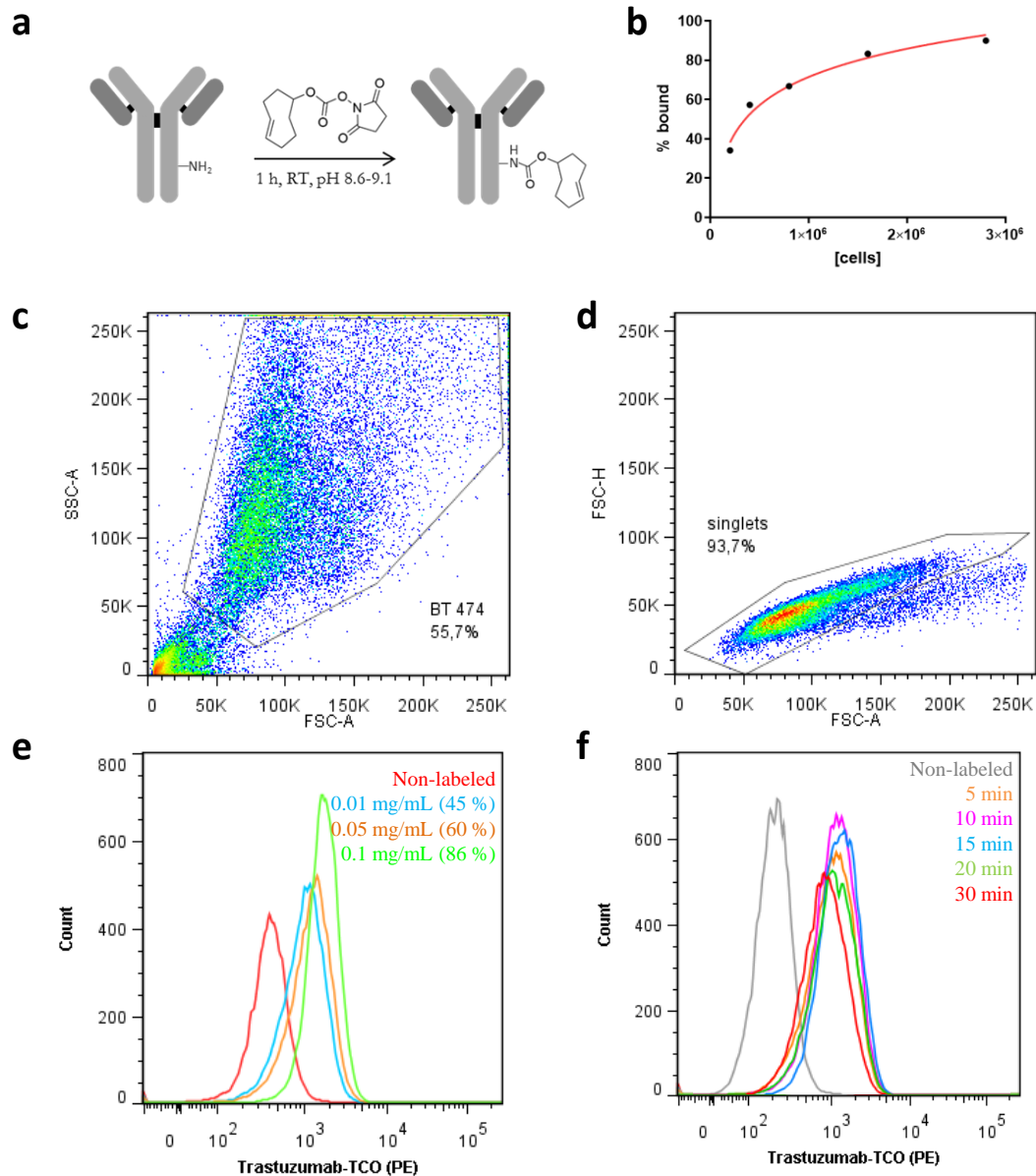### 2.1. Functionalization of the mAb Trastuzumab with TCO

Our studies were carried out in a breast cancer xenograft mouse model, generated by subcutaneous injection of human epidermal growth factor receptor (HER2) positive BT-474 cells in immunodeficient mice (see below). Hence, Trastuzumab, an antibody that selectively binds to HER2 and is clinically used to treat HER2$^+$ breast and stomach cancer,[15] was selected.

The selected antibody, Trastuzumab, was functionalized with a TCO ligand to enable the *in vivo* click reaction to the tetrazine-functionalized AuNPs. With that aim, the commercially available TCO-NHS was used and randomly conjugated to freely available amines of lysine residues in the antibody (Figure 2a). The conditions used (50-55 eq. excess of TCO-NHS with respect to the antibody, 60 min incubation at room temperature, $8.6 < pH < 9.1$, mAb concentration of 3 mg/mL) led to an average conjugate of about two TCO per mAb, as determined by photometric titration (see experimental section for details).

In order to ensure preserved binding capacity of the functionalized mAb, Lindmo assay[16] and flow cytometry studies based on fluorescence-activated cell sorting

7

(FACS) were carried out. The determined immunoreactive fraction by Lindmo assay was close to 90 % (Figure 2b), and flow cytometry experiments showed, with a concentration of 0.1 mg/mL and an incubation time of only 5 min, that over 80 % of cells carried Trastuzumab (Figure 2c-2f). Hence, both experiments revealed good mAb-receptor binding capacity after conjugation with TCO.


Figure 2: a) Illustration of the functionalization of the mAb with TCO-NHS by reaction with the free amino groups of lysine residues; b) Lindmo cell binding plot of

[89Zr]Trastuzumab on BT-474 cell; c-f) FACS studies, to monitor cell binding capability of TCO conjugated Trastuzumab; a) and b) gating strategy applied in the flow cytometry study: live cells were electronically gated based on the forward and side scatter parameter (a) and the not-single events leaved out based on forward area and height scatter parameters (b); c) and d) histogram of fluorescent BT-474 population with control (non-labeled): c) different concentrations of Trastuzumab (30 min incubation); d) different incubation times of Trastuzumab (0.1 mg/mL).

2.2. Synthesis, characterization and biocompatibility of gold nanoparticles

Previous studies carried out in our group with ^{124}I-labelled COSAN-functionalized gold nanoparticles with a core size of ca. 20 nm demonstrated high accumulation in organs with high presence of the MPS such as the liver and the spleen, together with low accumulation in the tumor probably due to low bioavailability.[10b] These results suggested that, in order to favor a fast clearance and prevent long residence time in these organs, there was the need to decrease particle core size. With this in mind, we decided in this study to prepare AuNPs with smaller core size. Additionally, the labeling strategy was also modified, as ^{124}I is an inconvenient radionuclide due to low availability. Based on previously reported works,[17] we decided to use a synthetic route enabling the incorporation of copper-64 (positron emitter, $t_{1/2}$ = 12.7 h) into the gold core, as this strategy was anticipated to guarantee radiochemical integrity of the AuNPs after intravenous administration. The approach consisted of synthesizing copper-alloyed particles (Figure 3a), as translation to radiolabeling conditions is straightforward by simple spiking stable copper with copper-64. Experimentally, a solution of chloroauric acid (HAuCl$_4$) and CuCl$_2$ in water was reduced with sodium borohydride (NaBH$_4$) and stabilized with thiolated amino-polyethylene glycol (HS-PEG$_{5k}$-NH$_2$). A color change could be observed during the addition of NaBH$_4$ from

the light yellow of HAuCl₄ to a dark red, as typically observed for AuNPs. After purification and washings, tetrazine moieties were anchored to the AuNPs surface, in order to enable pretargeting. With that aim, the NHS-activated ester, which readily reacts with free amino groups available at the terminus of the PEG chains, was used. Sufficient incorporation to yield subsequent click reaction was achieved (see below).
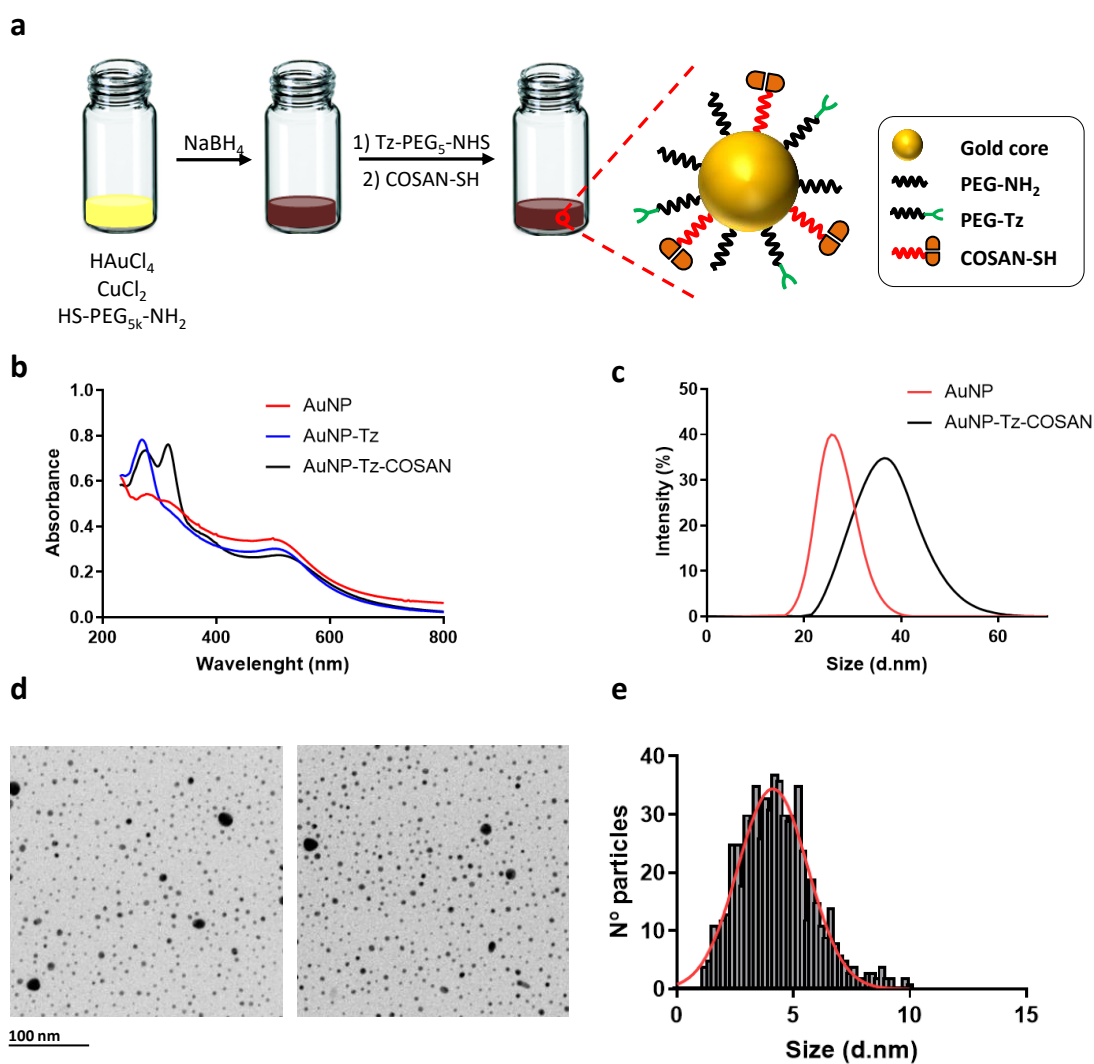
Figure 3: AuNPs synthesis and characterization: a) Schematic representation of synthesis and functionalization of AuNPs; b) UV-VIS spectra of the PEG-amine stabilized AuNPs core (red), functionalized with tetrazine (blue, max absorbance at 270 nm) and functionalized with tetrazine and COSAN (black, max absorbance at 315 nm); c) size distribution ranges as determined by DLS (intensity distribution);

red: non-functionalized, PEG-amine stabilized AuNPs; black: tetrazine- and COSAN-functionalized AuNPs; d) Representative TEM images to visualize shape and size of AuNPs; e) histogram of core diameter distribution (n = 670 particles). In red, the Gaussian curve fitted to experimental data.

The ultimate goal of our strategy was to design AuNPs with application in BNCT. The cobalt *bis*(dicarbollide) anion [3,3'-Co(C$_2$B$_9$H$_{11}$)$_2$]$^-$, commonly known as COSAN, and consisting of a central cobalt (Co^{3+}) atom sandwiched between two η^5-bonding [C$_2$B$_9$H$_{11}$]$_2^-$ moieties, was selected. The main reasons behind this selection were the remarkable thermal, kinetic, and photochemical stabilities,[18] the low toxicity both *in vitro* and *in vivo*,[19] and its previous use in the development of radiotherapeutics and BNCT agents.[20] In order to enable the attachment of COSAN on the surface of gold particles taking advantage of the thiol-gold chemistry, a thiolated derivative was synthesized as previously described.[10b] Efficient incorporation of COSAN on the AuNPs was achieved by one hour incubation at room temperature, as confirmed by combining different techniques (see below).

The multi-functionalized AuNPs were first characterized using UV-Vis spectrophotometry, which is an easy and straightforward method to monitor each step of the synthesis and functionalization of the particles. If the core of the AuNPs is formed correctly, the typical plasmon, dependent on shape and size of AuNPs, is visible. For the particles in hand the surface plasmon resonance was observed at ca. 500 nm (λ = 500 nm for AuNP; λ = 501 nm for Tz-functionalized AuNP; λ = 508 nm for Tz- and COSAN-functionalized AuNPs), as expected for AuNPs with average core diameter below 5 nm (Figure 3b). The incorporation of the COSAN and tetrazine

moieties was confirmed by the presence of additional peaks at ca. 315 and 270 nm, respectively (Figure 3b).

Transmission electron microscopy (TEM) analysis was carried out to determine core size and shape (Figure 3d). Spherical particles with a core size of 4.1 ± 1.5 nm were obtained. To determine the hydrodynamic diameter of the particles, dynamic light scattering (DLS) analysis was performed (Figure 3c). Intensity distribution curves showed a clear difference between the non-functionalized AuNPs and the COSAN- and tetrazine- functionalized particles, with an increase in the hydrodynamic diameter from 27.3 ± 4.0 to 39.6 ± 0.8 nm. The positive values obtained by zeta potential (ζ-potential) measurements of PEG-stabilized NPs in ultrapure water (7.9 ± 9.4 mV) confirm the presence of free amino groups on the surface. After coupling of tetrazine, which results in a decrease of the free amino groups present on the surface, and COSAN, which bears a net negative charge, zeta potential values of -33.6 ± 3.82 mV were obtained.

Finally, and in order to get additional experimental proof of the presence of boron clusters on the AuNPs, the composition was investigated by inductively coupled plasma mass spectrometry (ICP-MS) analysis. With that aim, the concentrations of gold, boron and cobalt were determined. Because each COSAN moiety contains one central cobalt atom sandwiched between two $[C_2B_9H_{11}]_2^-$ moieties, a boron to cobalt ratio of 18:1 was expected. ICP-MS analysis showed a ratio 18.2:1, thus confirming not only the presence of COSAN on the surface, but also its stability after attachment. Furthermore, the boron loading of the particles was determined to be 195 µg per mg gold, showing high boron loadings of the particles and thus suggesting favorable chemical composition for eventual BNCT applications.

After the successful synthesis, functionalization and characterization of the AuNPs, we experimentally proved the occurrence of the click reaction between the TCO functionalized Trastuzumab (TCO-mAb) and the tetrazine functionalized AuNPs. With that aim, agarose gel electrophoresis with a mixture of the two pretargeting components and respective controls was executed. The AuNPs derivatives were visible on the gel due to their red color. To visualize the mAb species after the electrophoresis, a staining of the gel with coomassie blue was performed. As control, each component was applied sole to the gel (Figure 4, lanes 1-2: Trastuzumab without and with TCO; lanes 6-7: AuNPs with and without tetrazine). Furthermore, a mix between either non-functionalized Trastuzumab and multifunctionalized AuNPs (Figure 4, lane 3) or functionalized Trastuzumab and AuNPs without tetrazine functionalization (Figure 4, lane 5) was applied. Good separation between the different species could be achieved. Additionally, the mixture of Trastuzumab-TCO and fully functionalized AuNPs (Figure 4, lane 4) showed a merged signal confirming the presence of both AuNPs and mAb, thus confirming that the click reaction took place.
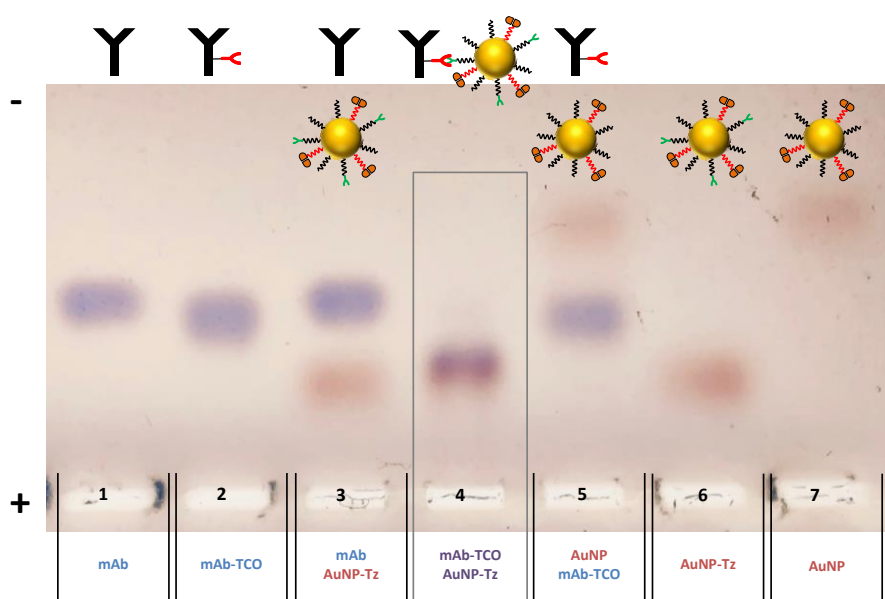
Figure 4: Representative image of agarose gel electrophoresis proving occurrence of click reaction. Lanes 1, 2, 6, and 7 present each component solo; lanes 3 and 5 are controls in which only one of the components is functionalized for the click reaction, and hence the click reaction is not occurring. The merged signal in lane 4 proofs the click reaction between the two fully functionalized components, the mAb-TCO and the multi-functionalized AuNPs..

Before moving to *in vivo* experiments, we evaluated the bio-compatibility of the multi-functionalized AuNPs. With that aim, cytotoxicity studies on BT-474 breast cancer cells were performed. The cells were treated with 5, 10, 20, 60, 80 and 120 µM (gold concentration) of AuNPs for up to 72 h. Analysis by standard MTT assay showed, with overall cell survivals over 90 %, no induced cell death due to the particles in BT-474 cells, indicating negligible cytotoxicity (Figure S1).

2.3. *In vivo* studies

We next moved to evaluate the suitability of the pretargeting strategy to accumulate boron atoms in the tumor. This strategy, using the same ligands but in a different NP type, has proven efficient to increase retention of the NPs in the tumor, confirming that the click reaction between the Trastuzumab-TCO and the tetrazine-functionalized NPs can occur *in vivo*.[12] First, and in order to be able to track the AuNPs *in vivo*, a positron emitting radionuclide was inserted. The possibility to synthesize copper alloyed AuNPs allows the incorporation of the radionuclide copper-64 in the core.[17] The synthesis of the radiolabeled particles was carried out following the procedure described as for the non-labeled particles, but $CuCl_2$ was spiked with radioactive $[^{64}Cu]CuCl_2$. To purify the AuNPs by spin filtration after the labeling, a 1 mM EDTA (ethylenediaminetetraacetic acid) solution was used to remove all loosely bound ^{64}Cu. Radio-thin layer chromatography (radio-TLC) studies after purification of the NPs

14

showed the presence of only one peak at the seeding spot, confirming thus the radiochemical purity of the labeled NPs (Figure S2). The radiochemical yield, calculated with respect to the starting amount of ^{64}Cu, was close to 10 %. Despite low, this value resulted in a sufficient amount of radioactivity to tackle subsequent *in vivo* studies. Furthermore, competitive stability tests showed that after 46 h at 37 °C in a 1 mM EDTA solution, 98 % of ^{64}Cu was still bound to the AuNPs, thus confirming that inclusion of the radionuclide into the crystal lattice of the gold core is an appropriate strategy (Figure S2).

To evaluate the amount of NPs accumulating in the tumor, immunocompromised NOD/SCID mice were inoculated subcutaneously with human BT-474 breast cancer cells, and the animals were randomly distributed in three groups. For all experiments fully functionalized and ^{64}Cu-radiolabeled AuNP were used (approximately 190 µg gold with 1-2 MBq per mouse). In case of the pretargeting group (G1, n = 4) 100 µg Trastuzumab-TCO per mouse was injected intravenously 24 h before the AuNPs. As control group (G2, n = 3) Trastuzumab without TCO conjugation was injected intravenously 24 h before the AuNPs. The last group, (G3, n = 4) also used as control, received only the administration of AuNPs.

PET-CT scans were performed approximately 1 h, 6 h, 24 h and 48 h post injection using the β- and X-cube micro system of Molecubes. We first analyzed the third group to evaluate the biodistribution and tumor uptake of the AuNPs alone. Visual inspection of the images (Figure 5a) confirmed that the particles show a rather typical distribution for spherical gold nanoparticles. However, quantification data (Figure 5b) showed a significant uptake in the liver and the spleen.. Yet, in organs such as the heart and the lungs, a steady decrease in the concentration of radioactivity can be observed over time, suggesting that the residence time of the NPs in blood is long.

This slow distribution and the accumulation in the liver suggest that our ultrasmall-sized AuNPs (core size ~4 nm) do not undergo renal clearance. This is, at first, surprising as it is known that small particles of below ca. 8 nm tend to follow renal clearance. However, the size of the particles increases due to the multifunctionalization; additionally, the hydrodynamic size is significantly larger (ca. 40 nm in diameter). This size is above the glomerular filtration, justifying the elimination route observed in our *in vivo* studies.

Maximum tumor uptake was achieved at t = 24 h post injection, with values of 4.76 ± 1.85 %ID/cm^3 (Figure 5c; Table S1), suggesting that there exists a passive accumulation of the NPs in the tumor, probably due to the EPR effect. A progressive, non-significant decrease in tumor uptake was observed afterwards (t = 48 h), which suggests the retention of the NPs in the tumor tissue. The tumor accumulation was clearly visualized in PET images when represented in axial view (Figure 5d).
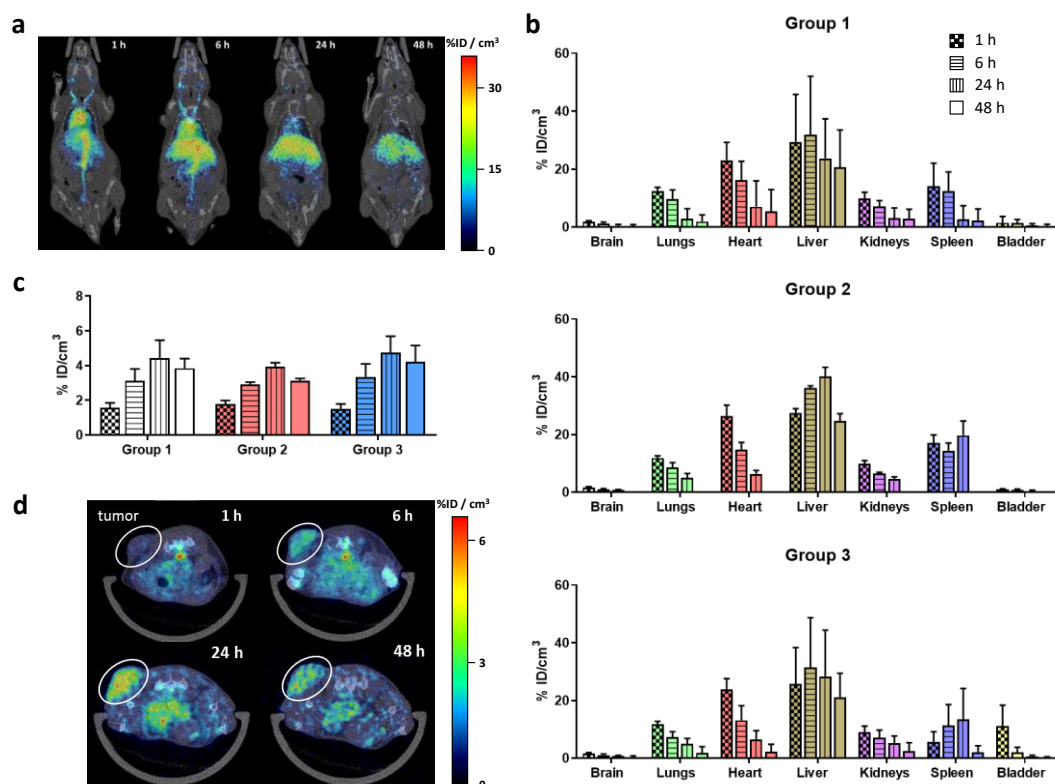
Figure 5: a) Representative PET images (maximum intensity projections, coronal views) obtained at different time points after intravenous administration of [^{64}Cu]AuNPs (group G3). All images have been co-registered with representative CT slices for localization of the radioactive signal; b) accumulation of multi-functionalized [^{64}Cu]AuNP in different organs at different time points after intravenous administration, analyzed by PET imaging, for groups G1, G2 and G3. Values are expressed as mean ± standard error mean; n = 4 for groups G1 and G3; n = 3 for group G2; c) tumor uptake of [^{64}Cu]AuNP in different experimental groups at different time points after administration. Values are expressed as mean ± standard error mean; n = 4 for groups G1 and G3; n = 3 for group G2; d) PET images (slices, axial view) showing local accumulation of the [^{64}Cu]AuNP (group G3) in the tumor at different times after administration. PET images have been co-registered with the corresponding CT slice for anatomical localization.

The analysis of the control (G2) and the pretargeting (G1) groups showed very similar biodistribution results at the whole body level (Figure 5b). Analyzing the tumor uptake, also very similar patterns were observed, with maximum uptake values of 4.42 ± 2.08 and 3.95 ± 0.38 % ID/cm^3 for groups G1 and G2, respectively (Figure 5c; Table S1). These results, which are statistically equivalent to those obtained for group G3, suggest that the pretargeting strategy does not have an effect on the accumulation and/or retention of the labeled particles in the tumor. Such counterintuitive results might be due to different reasons, including: (i) fast internalization of the mAb, which would decrease the amount of mAb on the cell surface and hence the amount of mAb-TCO available to undergo the click reaction with the Tz-functionalized AuNP; and

17

(ii) slow clearance of the AuNPs after accumulation in the tumor, due to fast cell internalization or limited drainage form the tumor tissue.

In order to gain further insight into the reasons behind the lack of significant differences between groups, we decided to carry out additional *in vitro* experiments. First, we investigated the cell internalization capacity of the nanoparticles in BT-474 cells. To perform the studies, the multi-functionalized AuNPs were fluorophore-labeled with TCO-Cy3 and incubated overnight with BT-474 cells. To visualize co-localization between the AuNPs and the lysosomes, the latter were stained with LysoTracker (deep red). The obtained images show a clear co-localization between the AuNPs and the lysosomes (Pearson's coefficient: r = 0.648; Manders' coefficients: M1 = 0.986, M2 = 0.972), confirming internalization after overnight incubation (Figure 6a). For most drug delivery agents in cancer therapy, cell internalization favors treatment efficacy, as the drug is usually more efficacious when delivered into the cell. In the particular case of BNCT, cell internalization is not strictly required, and the location of the boron-rich compound in the vicinity of cancer cells should be sufficient for the lithium and alpha particles to induce local damage. However, if the boron-rich compounds are located close to the cell nucleus, the amount of boron required to achieve equivalent therapeutic efficacy is lower. Hence, cell internalization of the NPs can be perceived as a positive result. Still, in our particular case, using a pretargeting strategy, the situation is different. In pretargeting, the NPs should initially accumulate in the tumor due to the EPR effect. After entering the tumor tissue, NPs should react with the mAb-TCO present at the cell surface, resulting in enhanced retention and/or internalization. Such enhanced tumor retention should be relevant only when, in the absence of pre-injection of mAb-TCO, the NPs are cleared from the tumor before internalizing. This, apparently, is not happening

with the gold nanoparticles used in the current study, leading to equivalent results for the three groups.

The second reason behind the lack of differences in our study could be the fast internalization of the mAb-TCO into cells. This is not expected to happen, as recently published results suggest that ca. 50% of the mAb-TCO is not internalized *in vivo* at t = 24 h after administration.[12] In any case, we decided to conduct further *in vitro* experiments to evaluate the pretargeting strategy between TCO-Trastuzumab and multi-functionalized AuNPs in cells. Therefore, the AuNPs were fluorophore-labeled with Cy3-NHS ester, which readily reacts with the PEG-amine functionalities of the particles. BT-474 cells were seeded in an 8-well plate (3×10^4 cells/well) and allowed to adhere overnight. Three different experimental groups were chosen and studied in parallel to enable comparison: (i) Trastuzumab-TCO + fully functionalized, Cy3-fluorophore labeled AuNPs (pretargeting); (ii) Trastuzumab non-functionalized + fully functionalized, Cy3-fluorophore labeled AuNPs (control 1); and (iii) fully functionalized, Cy3-fluorophore labeled AuNPs (no mAb; control 2). The mAb for group (i) and (ii) was incubated for 30 min at 37 °C. The media with unbound mAb was removed, the Cy3-fluorophore labeled AuNPs added to all groups and incubated for 10 or 30 min (see Fig. 6b for experimental set-up). The images of the different experimental groups, confirmed by the calculation of Pearson's and Manders' co-localization parameters (see Table S2), showed very similar cellular uptake of the fluorophore labeled AuNPs, but with an increased signal after 30 min incubation compared to the 10 min incubation (Figure 6c). We expected significant differences in the pretargeting experiment after 10 min incubation of the AuNPs. If the TCO functionalized Trastuzumab was available on the cell membrane and if the click reaction occurred, an intense signal on the cell membrane should have been visible,

which should decrease with longer incubation time due to internalization of the receptor-mAb-AuNP complex.[21] However, after 10 min incubation of the AuNPs, the fluorophore signal was low in all three cases and spread over the cell, co-localizing with the lysosomes, suggesting that internalization of the AuNP took place already. Hence, these results strongly suggest that the click reaction with Trastuzumab available at the cell surface and direct internalization of the AuNPs compete. However, the fast internalization of the AuNPs seems to be the main driving force for tumor retention. These results suggest that NPs with either lower cell internalization capacity or faster clearance from the tumor tissue are required in order to take advantage of the pre-targeting strategy. In our case, faster clearance might be achieved by decreasing hydrodynamic diameter. This should also contribute to decrease the accumulation in organs with high presence of the MPS, such as the liver.
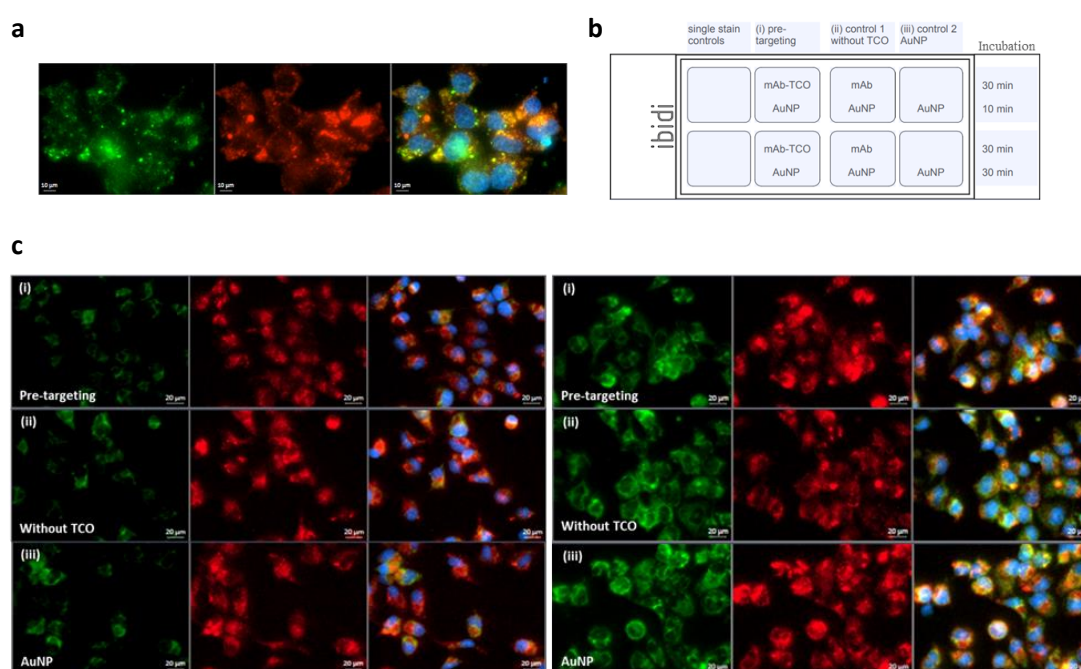
Figure 6: a) Representative image by live cell fluorescence microscopy of multi-functionalized AuNPs after overnight incubation in BT-474 cells. Green: AuNPs, fluorophore-labeled with TCO-Cy3; red: Lysosomes, stained with LysoTracker (deep red); blue: nucleus, stained with Hoechst 33342. Merged signals of different

fluorophores appear in yellow; b) 8-well plate with experimental set-up for pretargeting gold nanoparticles *in vitro*; c) representative images by fluorescence microscopy evaluating pretargeting AuNPs on BT-474 cells. As controls, incubation of AuNP alone (iii) and with non-functionalized Trastuzumab (ii) were performed. After 30 min incubation of mAb, incubation of AuNPs followed for either 10 min (left) or 30 min (right). Nucleus stained with Hoechst 33342 (blue), AuNPs with Cy3-NHS (green), lysosomes with LysoTracker (deep red). Merged signals of fluorophores appear in yellow.

3. Conclusions

In this work, we report on the synthesis, characterization and evaluation of spherical gold nanoparticles (AuNPs) loaded with the boron cluster COSAN and functionalized with tetrazine, to enable the click reaction with TCO-Trastuzumab and hence suitable for the pretargeting approach. Small-sized AuNPs with core diameter 4.1 ±1.5 nm were successfully synthesized, multi-functionalized and characterized. Stability of the functionalization and bio-compatibility was verified *in vitro*. Incorporation of the positron emitter ^{64}Cu was executed by synthesizing a copper alloyed gold core, enabling *in vivo* tracking of the AuNPs. Finally, it was confirmed by agarose gel electrophoresis that the two components, the Trastuzumab-TCO and the tetrazine-AuNPs, were able to undergo the click reaction *in vitro*.

In vivo studies in tumor-bearing animals confirmed accumulation of the NPs in the tumor with a maximum at t = 24 h after administration, when the NPs were administered alone. Pre-administration of the TCO-mAb did not result in an improved tumor accumulation or retention, probably due to the high internalization capacity of the AuNPs. Still, the significant tumor uptake of the AuNPs (4.8 ± 1.9 %ID/cm^3) and the high boron content (close to 20% with respect to gold) position small-sized gold

NPs as drug carriers with potential BNCT applications. However, the implementation of a successful pretargeting strategy may require faster-cleared particles to maintain tumor uptake while minimizing accumulation in major organs such as the liver.

4. Experimental section

4.1. Reagents

All reagents were of analytical grade and obtained from Sigma-Aldrich unless otherwise stated. Ultrapure water (resistivity 18.2 MΩ·cm at 25 °C) was obtained from a Milli-Q A10 Gradient equipment (Millipore). Cy3-NHS was purchased from BroadPharm and Cy3-TCO from AAT Bioquest. The antibody Trastuzumab was purchased from Roche Pharma, S.A. (Spain). [^{64}Cu]CuCl$_2$ (in 0.1 M HCl) was produced in house with an IBA Cyclone 18/9 cyclotron using a (p, n) reaction on a gold disk, electroplated with enriched nickel-64 and isolated with an ion exchange column following standard protocol.[22] BT-474 cells were purchased from ATCC. Animals were purchased from Charles River Laboratories France.

4.2. Instrumentation

UV-VIS spectra were measured in a Jasco V630BIO Spectrophotometer or in NanoDrop® ND-1000 V3.5.2. Microscopy experiments were carried out using a Zeiss Axio Observer Fluorescence microscope and ibidi clear bottomed µ-slide 8-well microscopy plates. Images were analyzed by ZEN2012-ZEISS software.

Transmission electron microscopy (TEM) was performed using a JEOL JEM-1400 plus microscope (Jeol, Tokyo, Japan) working at 120 kV. The carbon film of copper grids (CF400-Cu) was treated under air plasma in a glow discharge system (K100X, Emitech, Kent, UK, 40 mA during 2 min) just before sample preparation. For TEM examinations, a single drop (1 µL) of the NPs solution was placed onto a copper grid

coated with a carbon film (Electron Microscopy Sciences, Hatfieled, PA, USA). After 1 min, the drop was removed with filter paper and the sample was incubated with 3 µL of uranyl acetate 0.5% (3 min). For the determination of particle size and generation of the histograms, particle analysis toolbox in ImageJ (version 1.51w) was used. TEM images were binarized using an optimized threshold and subjected to hole-filling and water-shedding. Diameter (Feret's Statistical Diameter) of each individual particle (n = 670) was determined.

Inductively coupled plasma mass spectrometry (ICP-MS) measurements were performed on a Thermo iCAP Q ICP-MS (Thermo Fisher ScientificGmbH, Bremen, Germany). An ASX-560 autosampler was coupled to the ICP-MS (CETAC Tech, Omaha, NE, USA).

Dynamic light scattering (DLS) and zeta-potential measurements were performed using a Malvern Zetasizer Nano ZS system (Malvern Instruments, Malvern, UK). The particle size measurement settings were: 3 measurements/14 runs/10s in scattered mode at 173° angle. Measurements were conducted at T = 25 °C and neutral pH.

Radio-thin layer chromatography (radio-TLC) was performed using iTLC-SG chromatography paper (Agilent Technologies, CA, USA) and 20 mM citric acid + 60 mM EDTA/acetonitrile solution (9/1 v/v) as the stationary and mobile phases, respectively. TLC plates were analyzed using a TLC-reader (MiniGITA, Raytest).

4.3. Chemistry and radiochemistry

4.3.1. Conjugation of TCO-NHS to mAb

The monoclonal antibody (mAb) Trastuzumab (21 mg/mL, 2 mg) was diluted with PBS (phosphate-buffered saline, 10 mM, pH 7.4) to a concentration of 3.0 mg/mL. The pH was adjusted to 8.6–9.1 with 0.1 M Na_2CO_3. *Trans*-Cyclooctene (TCO-NHS, 20 mM in DMSO, 26 µL, 50–55 eq.) was added. After incubation (120 min, room

temperature) non-reacted TCO-NHS was removed by spin filtration (100 kDa, 16128 g) and the conjugated mAb washed three times with PBS (pH 7.4). After recovering the mAb from the filter with PBS its concentration was determined by NanoDrop®, using the default extinction coefficient for immunoglobulin type mAbs: $\varepsilon(mAb) = 210$ L/(mmol x cm).

4.3.2. TCO conjugation –photometric titration analysis

To an aliquot of the TCO-conjugated mAb (0.05 mg; 0.3 nmol) was added 6-methyl-tetrazine-sulfo-Cy3 (mTzCy3, 1 mg/mL in DMSO; 1:6 with respect to the initial amount of TCO-NHS). After 5 min incubation at room temperature, the fluorophore-labeled mAb was purified by spin filtration (100 kDa, 16128 g) and washed four times with PBS. After recovering the mAb/TCO/mTzCy3 from the filter with PBS, the concentrations of mAb and mTzCy3 were determined by NanoDrop®, using the extinction coefficients: $\varepsilon(mAb) = 210$ L/(mmol $\times$ cm), NanoDrop® default for immunoglobulin type mAbs; and $\varepsilon(mTzCy3) = 151$ L/(mmol $\times$ cm), taken from datasheet of Jena Bioscience. The experiments were performed in duplicates.

4.3.3. Synthesis of AuNPs

For the synthesis of AuNPs the protocol reported by Zhao et al. was used [17], with minor modifications. In brief, ultrapure water (0.9 mL) was mixed with aqueous $HAuCl_4$ (10 µL, 100 mM; 0.4 mg, 1 eq.), aqueous $CuCl_2$ (10 µL, 10 mM; 0.1 mg, 1 eq.) and aqueous NH_2-PEG$_{5k}$-SH (25 µL, 10 mM; 2.5 mg, 0.25 eq.) in a 10 mL glass vial. Under vigorous stirring, freshly prepared aqueous $NaBH_4$ solution (100 µL, 40 mM; 0.2 mg, 4 eq) was added drop wise. After 2 min, the stirring was stopped and the particles were allowed to settle for 2 h at room temperature. Purification was performed by spin filtration (30 kDa, 16128 g) including 3 washings with PBS (pH 7.4) and the particles were recovered from the filter in PBS (400 µL). Subsequently,

COSAN-SH solution in ethanol (13 µL, 20 mM; 0.1 mg, 0.25 eq) was added and the mixture was incubated for 1 h at room temperature. After purification via spin filter as described above, the pH of the suspension was adjusted to 8 - 9 with 0.1 M NaOH and Tz-PEG$_5$-NHS (25 µL, 20 mM in DMSO; 0.3 mg, 0.5 eq) was added. After 1 h incubation at room temperature the particles were purified by spin filtration (30 kDa, 16128 g), washed three times with PBS and finally recovered in 400 µL PBS. In all cases, UV-VIS analysis was performed after each washing, to ensure that the ratio between the intensity of the bands corresponding to the plasmon and the ligand (i.e. COSAN or tetrazine) remained constant, ensuring thus the absence of free ligand. Characterization of the final particles was carried out using UV-VIS spectrophotometry, DLS, zeta-potential, ICP-MS and TEM.

4.3.4. *Fluorophore-labeling of AuNPs with TCO-Cy3*

The multifunctionalized AuNPs (450 µL in PBS, 0.2 mg/mL) were incubated with 3 µL TCO-Cy3 (10 mM in DMSO) for 5 min at room temperature. The particles were purified by spin filtration (30 kDa) and recovered in PBS. The labeling was confirmed by UV-VIS spectra.

4.3.5. *Fluorophore-labeling of AuNP with Cy3-NHS*

The multifunctionalized AuNPs (450 µL in PBS, 0.2 mg/mL) were adjusted with 0.1 M NaOH to pH 8.6-8.9 and Cy3-NHS (5 µL, 1 mg/mL in DMSO) was added. After 1 h incubation at room temperature particles were purified by spin filtration (30 kDa) and recovered in PBS. The labeling was confirmed by UV-VIS spectrophotometry.

4.3.6. *Gel electrophoresis*

A 1.5 % agarose gel was prepared following standard protocol. In brief, agarose (1.5 g) was suspended in Tris-Borate-EDTA (TBE) buffer (100 mL) and heated until it

almost reached its boiling point. The solution was poured in a gel chamber, the comb placed and let settle to polymerize. Samples were prepared in 20 µL aqueous batches, including 5 µL loading buffer. Samples (10 µL each) were loaded on the gel and run for approximately 1 h at 100 V. Visualization of the antibody on the gel was achieved by incubation in coomassie blue (1 h), followed by 2 days in de-staining solution to reduce the background staining.

4.3.7. Synthesis of radiolabeled AuNPs

The synthesis of ^{64}Cu-labeled AuNPs was carried out following a previously reported method, with minor modifications.[17] In brief, ultrapure water (0.9 mL) was mixed with aqueous $HAuCl_4$ (10 µL, 100 mM; 0.4 mg, 1 eq.), [^{64}Cu]$CuCl_2$ solution in 0.1 M HCl (10 µL, 92.5 MBq; neutralized with an equivalent volume of 0.1M NaOH) and aqueous NH_2-PEG_{5k}-SH (25 µL, 10 mM; 2.5 mg, 0.25 eq.) in a 10 mL glass vial. Under vigorous stirring, freshly prepared aqueous $NaBH_4$ (100 µL, 40 mM; 0.2 mg, 4 eq.) was added drop-wise. After 2 min, the stirring was stopped and the particles were allowed to settle for 2 h at room temperature. Purification was performed by spin filtration (30 kDa, 16128 g) including 3 washings with 1 mM EDTA, and the particles were recovered from the filter in 400 µL PBS. The radiolabeling efficiency and radiochemical purity were monitored by instant thin layer chromatography (iTLC) using 20 mM citric acid + 60 mM EDTA as the mobile phase; Rf(AuNP) = 0, Rf(^{64}Cu-EDTA) = 0.5. Subsequently, COSAN-SH solution in ethanol (13 µL, 20 mM; 0.1 mg, 0.25 eq.) was added and the mixture was incubated for 1 h at room temperature. After purification via spin filter as described above, the pH of the AuNP suspension was adjusted to 7.8 – 8.8 with 0.1 M NaOH and Tz-PEG_5-NHS (25 µL, 20 mM in DMSO; 0.3 mg, 0.5 eq.) was added. After 1 h incubation at room temperature the particles were purified by spin filtration and recovered in 400 µL PBS.

4.4. *In vitro* studies

4.4.1. *Cells*

BT-474 cells were cultured in DMEM medium (Gibco), supplemented with 10% fetal bovine serum (FBS) and 1 % penicillin-streptomycin, at 37 °C with 5 % CO_2 in a humid atmosphere. Cells were confirmed to be free of mycoplasma contamination using the MycoAlert[TM] detection kit (Lonza).

4.4.2. *Lindmo assay*

The assay was performed using the protocol of Lindmo.[16] The binding assay for Trastuzumab was set up using one concentration of mAb (15 ng/mL) and different dilutions of 0.5 mL BT-474 cells in PBS/1%BSA (2.8–0.2 × 10^6 cells/mL) in triplicates. The lowest concentration was prepared twice, the second set serving as non-specific binding (NSB) control (containing 2 µL of 5 mg/mL non-labeled mAb). To each cell dilution, radiolabeled Trastuzumab (0.5 mL) was added and incubated in a head over head rotator at 4 °C overnight. The cell suspensions were centrifuged, the supernatant (500 µL) separated and all samples (pellets and supernatants) measured in a gamma-counter. The activity measured from the supernatants was subtracted from the pellet activity to calculate the immunoreactive fraction.

4.4.3. *Flow cytometry study with Trastuzumab-TCO-mTzCy3*

TCO conjugated Trastuzumab was fluorophore-labeled with 6-methyl-tetrazine-sulfo-Cy3 (mTzCy3) via click reaction. BT-474 cells were seeded in a 24-well plate (5×10^5 cells/well) and incubated overnight to adhere (37 °C, 5% CO_2). The media was removed and 0.5 mL fresh media was added to non-labeled and viability control wells. To the other wells, 0.5 mL of Cy3-fluorophore-labelled Trastuzumab (0.1, 0.05 or 0.01 mg/mL) were added. The incubation (5, 10, 15, 20 and 30 min) at room temperature was stopped by removing the media and detaching cells with trypsin. The

suspensions were transferred into FACS tubes, centrifuged, the supernatant removed and resuspended in 0.5 mL PBS. 0.1 mL of viability dye (Zombie NIR, Molecular Probes) was added to all samples (except non-labeled control) and incubated for 15-30 min at room temperature. The samples were washed with FACS buffer (10 mM PBS/1%BSA) via centrifugation and resuspended in 0.2 mL for flow cytometry measurements.

4.4.4. Cytotoxicity studies of AuNPs

To determine cell viability, BT-474 human breast cancer cells were incubated with multifunctionalized AuNPs over 24 h, 48 h and 72 h. Cells were seeded $(3 \times 10^4$ cells/well, 100 µL/well, 96-well plate), allowed to adhere overnight in complete media and maintained in a humid atmosphere at 37 °C and 5% CO_2. Then, media was removed and cells were left untreated (control) or incubated with the AuNP-containing formulations, diluted accordingly in media. After the desired time, cell supernatant was removed and MTT reagent (100 µL/well; Roche), diluted in the corresponding media to the final concentration of 0.25 mg/mL, was added. After 1 h incubation at 37 °C and 5% CO_2, the excess reagent was removed and formazan crystals were solubilized by adding DMSO (200 µL/well). The optical density of each well was measured in a TECAN Genios Pro 96/384 microplate reader at 550 nm. Data was represented as the percentage of cell survival (mean ± standard error mean, n = 6) compared to control wells.

4.4.5. In vitro internalizing studies of AuNP-Tz-TCOCy3

BT-474 cells were seeded in a poly-L-Lysine treated ibidi µ-slide 8-well plate $(3 \times 10^4$ cells/well in 0.3 mL) and incubated overnight to adhere (37 °C, 5% CO_2, humid atmosphere). The media was removed and 0.1 mL Hoechst 33342 (1 µg/mL in media) added to stain the nucleus. After 10 min incubation (37 °C, 5% CO_2, humid

atmosphere) 0.1 mL LysoTracker^{TM} Deep Red (1 µg/mL in media; Invitrogen) was added to stain the lysosomes. After 20 min incubation (37 °C, 5% CO_2, humid atmosphere) media was removed and 0.3 mL of Cy3-labeled AuNP (20 µg/mL in media) added. After incubation overnight (37 °C, 5% CO_2, humid atmosphere) the media was removed and replaced with fresh media. The images were taken with a Cell Axio Observer Fluorescence Microscope. Controls of single staining for each fluorophore were included. Images were analyzed with ZEN2012-ZEISS software and Pearson's and Manders' co-localization parameters were calculated using ImageJ software including JACoP plugin.[23]

4.4.6. In vitro pretargeting studies of Trastuzumab-TCO and Cy3-AuNP-Tz

BT-474 cells were seeded in an ibidi µ-slide 8-well plate as described in the previous section. After staining of the nucleus and the lysosomes with Hoechst 33342 and LysoTracker^{TM} Deep Red respectively, media was removed and 0.1 mL Trastuzumab-TCO (1.0 µM) added. After 30 min incubation (37 °C, 5% CO_2, humid atmosphere) the media was removed and 0.3 mL of Cy3-labeled AuNP (20 µg/mL in medium) added. Incubation was done for 10 min or 30 min (37 °C, 5% CO_2, humid atmosphere), the media removed and replaced with fresh media. The images were taken with a Cell Axio Observer Fluorescence Microscope. Controls of single staining for each fluorophore were included. Images were analyzed by ZEN2012-ZEISS software.

4.5. *In vivo* studies

4.5.1. Animals

All animal experiments were performed in accordance with the Spanish policy for animal protection (RD53/2013), which meets the requirements of the European Union directive 2010/63/UE regarding the protection of animals used in experimental

procedures. All experimental procedures were approved by the Ethical Committee of CIC biomaGUNE and authorized by the local authorities (Diputación Foral de Gipuzkoa; project code: PRO-AE-SS-091). All animals were housed in ventilated cages and fed on a standard diet ad libitum. The studies were performed on female NOD.CB17-*Prkdc^{scid}*/NCrCrl (NOD/SCID) mice.

4.5.2. PET imaging studies

To obtain the BT-474 breast cancer xenograft model, NOD/SCID mice were implanted with 0.72 mg, 60-day release, 17β-estradiol pellets (E2-M/60, Belma Technologies). One day later, 10^7 BT-474 cells were subcutaneously inoculated using a 25-gauge needle in the back of each mouse. Cells were diluted in Matrigel® matrix (Corning) at a final volume of 0.2 mL (1:1 ratio between cell and Matrigel). Tumor growth was monitored by serially measuring the diameters with an electronic caliper and calculating the tumor volumes by the formula: volume = width^2 × length / 2. Once tumors reached approximately a volume of 300 mm^3, animals were randomly divided in three groups (G1 and G3: n = 4, G2: n = 3). For the pretargeting group (G1) TCO functionalized Trastuzumab (ca. 100 µg, 1 µg/µL) was intravenously injected via tail vein. The control group (G2) received an intravenous injection with the same amount of non-functionalized Trastuzumab. 24 h post injection of TCO-mAb (G1) or mAb (G2), multifunctionalized and ^{64}Cu-radiolabeled AuNPs (200 µg gold in 100 µL PBS with 1-2 MBq per mouse) were injected intravenously. The same amount was injected to the third group (G3) which did not receive Trastuzumab beforehand. Imaging studies were conducted using positron emission tomography (PET) in combination with computed tomography (CT), using the β- and X-cube micro system of Molecubes. Static whole-body images (1 bed) were acquired in a 511 keV ± 30 % energetic window at 1 h, 6 h, 24 h and 48 h post injection

(acquisition time 20 min for 1 h and 6 h, 45 min for 24 h and 60 min for 48 h). PET images were analyzed using PMOD image analysis software (PMOD Technologies Ltd, Zürich, Switzerland). Volumes of interest (VOIs) were manually delineated in the different organs, and the concentration of radioactivity was determined. Values were finally expressed percentage of injected dose per cubic centimeter (%ID/cm^3; mean ± standard deviation).

4.6. Statistical analysis

Statistical significance of differences in between methods was calculated using 2-way ANOVA followed by Tukey's test for multiple comparisons. Differences were concluded significant for P values < 0.05. Statistical tests were performed using GraphPad Prism 7.03 (GraphPad Software, La Jolla, CA).

Acknowledgements

Conflict of interest

The authors have declared that no competing interest exists

References

1.   L. Lin, L. Yan, Y. Liu *et al*, *Journal of Hematology and Oncology* **2019**, *12*.

2.   G. L. Locher, *American Journal of Roentgenology, Radium Therapy* **1936**, *36*, 1.

3.   R. F. Barth, J. A. Coderre, M. G. H. Vicente, T. E. Blue, *Clin. Cancer Res.* **2005**, *11*, 3987.

4.   W. A. G. Sauerwein, P. M. Bet, A. Wittig: Drugs for BNCT: BSH and BPA. In: *Neutron Capture Therapy: Principles and Applications. Volume 9783642313349*, edn.; 2012: 117.

5.   a) T. Mitsumoto, S. Yajima, H. Tsutsui *et al*: Cyclotron-based neutron source for BNCT. In: *AIP Conference Proceedings: 2013*; 2013: 319; b) T. Kato, K. Hirose, H. Tanaka *et al*, *Appl. Radiat. Isot.* **2020**, *156*.

6.   a) P. J. Kueffer, C. A. Maitz, A. A. Khan *et al*, *Proc. Natl. Acad. Sci. U. S. A.* **2013**, *110*, 6512; b) T. O. B. Olusanya, G. Calabrese, D. G. Fatouros *et al*, *Biophys. Chem.* **2019**, *247*, 25; c) M. J. Luderer, B. Muz, K. Alhallak *et al*, *Pharm. Res.* **2019**, *36*; d) W. Lee, S. Sarkar, H. Ahn *et al*, *Biochem. Biophys. Res. Commun.* **2020**, *522*, 669.

7.   a) R. Tietze, H. Unterweger, S. Dürr *et al*, *Appl. Radiat. Isot.* **2015**, *106*, 151; b) E. Oleshkevich, A. Morancho, A. Saha *et al*, *Nanomedicine: Nanotechnology, Biology, and Medicine* **2019**, *20*; c) O. Icten, D. A. Kose, S. J. Matissek *et al*, *Mater. Sci. Eng., C* **2018**, *92*, 317.

8.   M. Yamagami, T. Tajima, K. Ishimoto *et al*, *Heteroat. Chem* **2018**, *29*.

9.   T. H. Ferreira, M. C. Miranda, Z. Rocha *et al*, *Nanomaterials* **2017**, *7*.

10.   a) C. Y. Wu, J. J. Lin, W. Y. Chang *et al*, *Colloids Surf. B. Biointerfaces* **2019**, *183*; b) K. R. Pulagam, K. B. Gona, V. Gómez-Vallejo *et al*, *Molecules* **2019**, *24*.

11.   M. Longmire, P. L. Choyke, H. Kobayashi, *Nanomedicine* **2008**, *3*, 703.

12.   I. V. J. Feiner, K. R. Pulagam, C. Simó *et al*, *Submitted* **2020**.

13.   A. Rondon, F. Degoul, *Bioconjugate Chem.* **2020**, *31*, 159.

14.   a) H.-H. Jeong, E. Choi, E. Ellis, T.-C. Lee, *Journal of Materials Chemistry B* **2019**, *7*, 3480; b) N. Elahi, M. Kamali, M. H. Baghersad, *Talanta* **2018**, *184*, 537.

15.   C. A. Hudis, *N. Engl. J. Med.* **2007**, *357*, 39.

16.   T. Lindmo, E. Boven, F. Cuttitta *et al*, *J. Immunol. Methods* **1984**, *72*, 77.

17.   Y. Zhao, D. Sultan, L. Detering *et al*, *Nanoscale* **2014**, *6*, 13501.

18.   B. P. Dash, R. Satapathy, B. R. Swain *et al*, *J. Organomet. Chem.* **2017**, *849-850*, 170.

19.   a) I. Fuentes, T. García-Mendiola, S. Sato *et al*, *Chemistry – A European Journal* **2018**, *24*, 17239; b) R. A. Spryshkova, L. I. Karaseva, V. A. Bratsev, N. G. Serebryakov, *Meditsinskaya Radiologiya* **1981**, *26*, 62.

20.   a) M. F. Hawthorne, A. Maderna, *Chem. Rev.* **1999**, *99*, 3421; b) M. Gozzi, B. Schwarze, E. Hey-Hawkins, *Pure Appl. Chem.* **2019**, *91*, 563.

21.   S. Hapuarachchige, Y. Kato, D. Artemov, *Scientific Reports* **2016**, *6*, 24298.

22.   P. Burke, O. Golovko, J. C. Clark, F. I. Aigbirhio, *Inorg. Chim. Acta* **2010**, *363*, 1316.

23.   S. Bolte, F. P. CordeliÈRes, *J. Microsc.* **2006**, *224*, 213.